MAX-PLANCK-INSTITUT FÜR PLASMAPHYSIK

GARCHING BEI MÜNCHEN

A Nonlinear Resistive MHD - Code in Cylindrical Geometry

A. JAKOBY

IPP 6/269 November 1987

Die nachstehende Arbeit wurde im Rahmen des Vertrages zwischen dem Max-Planck-Institut für Plasmaphysik und der Europäischen Atomgemeinschaft über die Zusammenarbeit auf dem Gebiete der Plasmaphysik durchgeführt.

A NONLINEAR RESISTIVE MHD - CODE IN CYLINDRICAL GEOMETRY

A. JAKOBY

Max-Planck-Institut für Plasmaphysik, EURATOM Association

Garching bei München, FRG

Abstract

A computer code has been developed which solves the full compressible resistive magnetohydrodynamic (MHD) equations in cylindrical geometry. The variables are expanded in Fourier series in the poloidal and axial directions while finite differences are used in the radial direction. The time advance is accomplished by using a semi-implicit predictor-corrector-scheme. Applications to the ideal m=1 ideal kink saturation in the nonlinear regime and the subsequent decay of the singular current layer due to resisivity are presented.

1. INTRODUCTION

In magnetic fusion research the magnetohydrodynamic (MHD) equations are widely used and successful in describing the macroscopic behavior of fusion plasmas. The MHD fluid model is used for studying the macroscopic stability, the equilibrium properties and the gross nonlinear dynamics of the plasma fluid.

Progress in computertechnologie and in the numerical methods allow to solve the full MHD tokamak problem in cylindrical geometry with approximatly the same effort as was commonplace when the reduced tokamak equations were the only possible set of equations which could reasonably be treated with. Thus large scale MHD calculations involving up to eight coupled nonlinear partial differential equations are usual today.

In magnetic fusion research it has been established that instabilities tend to develop singularities or large gradients in radial direction nonlinearily, so using Fourier expansion in poloidal and axial directions, finite differences in radial direction have proven to be an efficient method. This is because of the periodic nature of poloidal and axial directions in most fusion devices.

In this paper we describe a computer code solving the full set of MHD equations as an initial-boundary-value problem using such a Fourier decomposition combined with finite differences. The geometry used is cylindrical (r, θ, z) but because of the periodic boundary conditions in z the cylinder is topologically equivalent to a torus. All effects which are not correlated to toroidal curvature can therefore be treated with our code.

This code is based on an earlier and preliminary MHD code which was written by Biskamp and co-workers. The code described here is an extended and refined version of this Biskamp code.

The paper is organized as follows. Section 2 presents the mathematical model and discusses various assumptions which have to be made. In section 3 the numerical method is explained and section 4 discusses the performance of the code by doing some test calculations. Section 4 also presents a nonlinear physical application.

2. MATHEMATICAL MODEL

2.1 The Equations

On the macroscopic scale the plasma may be described as an electrically conducting fluid in a magnetic field. The behavior of the plasma in this model is adequately described by the single fluid resistive MHD equations. In suitable nondimensional form they read:

$$\rho(\frac{\partial \mathbf{V}}{\partial t} + \mathbf{V} \cdot \nabla \mathbf{V}) = -\nabla P + (\nabla \times \mathbf{B}) \times \mathbf{B}, \tag{2.1}$$

$$\frac{\partial \mathbf{B}}{\partial t} = \nabla \times (\mathbf{V} \times \mathbf{B}) - \nabla \times (\eta \nabla \times \mathbf{B}), \tag{2.2}$$

$$\frac{\partial \rho}{\partial t} = -\nabla \cdot (\rho \mathbf{V}), \tag{2.3}$$

$$\frac{\partial P}{\partial t} = -\gamma P \nabla \cdot \mathbf{V} - \mathbf{V} \cdot \nabla P + \frac{2}{3}\eta (\nabla \times \mathbf{B})^2, \tag{2.4}$$

together with

$$\nabla \cdot \mathbf{B} = 0 \tag{2.5}$$

$$\eta \mathbf{j} = \mathbf{E} + \mathbf{V} \times \mathbf{B}. \tag{2.6}$$

With the definitions: ρ: density, $\mathbf{V}$: velocity of the fluid, $\mathbf{B}$: magnetic field, P: Pressure, $\mathbf{j}$: plasmacurrent, η: plasmaresistivity, γ: adiabatic coefficient.

To obtain this nondimensional form of the equations the following transformations were made:

$$\frac{t}{t_A} \to t, \ \frac{r}{a} \to r, \ a\nabla \to \nabla, \ \frac{\mathbf{V}}{V_A} \to \mathbf{V},$$

$$\frac{\mathbf{B}}{B^z(0)} \to \mathbf{B}, \ \frac{4a\pi}{B^z(0)}\mathbf{j} \to \mathbf{j}, \ \frac{\rho}{\rho(0)} \to \rho,$$

$$\frac{4\pi}{(B^z(0))^2} P \to P, \ \frac{c^2}{4\pi a V_A} \eta \to \eta \ ,$$

with $\tau_A = \frac{a}{V_A}$ (Alfvéntime) and $V_A = \frac{B^z(0)}{\sqrt{4\pi\rho(0)}}$ (Alfvénvelocity). This means that the time is measured in units of τ_A where a is the minor radius of the torus.

For JET parameters $a = 1.23\ m,\ B^z = 2.9\ T,\ n = 1.6 \cdot 10^{19}$ one obtains $\tau_A \approx 0.15 \mu s$.

2.2. Physical Assumptions

2.2.1. *Density ρ*

In this paper we make the following assumptions:

$$\rho = 1 \tag{2.7}$$

which means that we drop the equation (2.3).

2.2.2. *Resistivity η*

The resistivity η is not considered a fully dynamic variable which is dynamically evolved through an extra equation. It is assumed that η is just a function of the radial coordinate r and especally not a function of time:

$$\eta = \eta(r)$$

The main feature of $\eta \neq 0$ is the fact that some topological constraints are no longer valid. The assumption $\eta \neq 0$ creates qualitativly new physics (tearing modes, reconnection). For most applications the assumption $\eta = \eta(r)$ is therefor fully justified.

In this work η is defined as

$$\eta = \eta(r) = \frac{\eta^0}{j_0^z},$$

with j_0^z being the equlibrium current in z-direction.

2.2.3. *Dissipation*

The plasma with $\eta \neq 0$ defines a dissipative dynamical system. The qualitativly new physics mentioned in paragraph 2.2.2 enters via equation (2.2) and the Ohmic heating

$$\eta \mathbf{j}^2 = \eta\ (\nabla \times \mathbf{B})^2$$

in equation (2.4) can be neglected in lowest order in the fluid picture

$$\sqrt{|\mathbf{V}|^2} = v \quad << 1$$

$$\frac{|\mathbf{E}|}{|\mathbf{B}|} = \alpha \quad << 1 \, .$$

One obtains

$$\mathrm{j}^2 = (\nabla \times \mathbf{B})^2 \sim \mathbf{E}^2 + v^2\mathbf{B}^2 + 2\mathbf{E} \cdot \mathbf{B}v.$$

which means

$$\mathrm{j}^2 \sim (\alpha^2 + v^2 + \alpha v)\mathbf{B}^2.$$

This second order term is neglected in the further study.

2.2.4. *Geometry*

Our code solves the MHD equations (2.1)-(2.4) in cylindrical geometrie (r, θ, z). In fusion theory this is only an approximation to the large toroidal devices such as ASDEX or JET. Due to the periodic boundary conditions in z-direction we can simulate these devices and the physics involved as long as problems are treated which do not depend on toroidal curvature.

Another argument for choosing the more simple cylindrical geometry is the fact that nonlinear physics is still a vast field where intense research is necessary and effects very carefully have to be examined in order to provide sound material for futher analytical studies. For this purpose the geometry should be as simple as possible. Cylindrical geometry thus provides both the possibility of simulating experimental devices and an easy enough geometry where nonlinear analytic results may be possible.

3. NUMERICAL METHODS

3.1. Spatial Discretization

Due to the periodic nature of the poloidal and axial directions in most fusion devices we

assume the following expansion of all variables:

$$f(r,\theta,z;t) = \sum_{m,n} f_{mn}(r;t)\ e^{i(m\theta+\frac{n}{R}z)} \tag{3.1}$$

In radial direction we use finite differences. The Fourier coefficients $f_{mn}(r;t)$ are then advanced in time. The discretization in r should fulfill two conditions:

1. The origin ($r = 0$) and the outer boundary conditions ($r = 1$) should be easy to implement.
2. It should be possible to impose the divergence condition $\nabla \cdot \mathbf{B} = 0$ as an initial-value condition.

3.1.1 *Grid*

The easiest way to fulfill conditions 1., 2. is to use a *staggered mesh.* There, some quantities are defined at the gridpoints x_i (cellboundaries), the others are defined at the cellcenters $x_{i+1/2}$.

At the gridpoints x_i one defines:

$$B^r\ ,\ V^r\ ,\ j^\theta\ ,\ j^z\ . \tag{3.2a}$$

At the cellcenters $x_{i+1/2}$ one defines:

$$B^\theta\ ,\ B^z\ ,\ V^\theta\ ,\ V^z\ ,\ P\ ,\ j^r\ . \tag{3.2b}$$

Normalising in r-direction one obtains

$$0 \le r \le 1,$$

for the cellboundaries

$$0 = x_0 \le r \le x_N = 1\ , \tag{3.3}$$

and for the cellcenters

$$0 < x_{1/2} \leq r \leq x_{N-1/2} < 1, \tag{3.3}$$

with N the number of gridpoints.

Quantities which are defined at the cellboundaries x_i (the cellcenters $x_{i+1/2}$) can be calculated if needed at the cellcenters $x_{i+1/2}$ (cellboundaries x_i) by simple averages as in the following example:

B^r is defined at gridpoints x_i, $B^r(r = x_i) = B_i^r$ and if $B^r(r = x_{i+1/2})$ is needed one averages

$$B^r(r = x_{i+1/2}) = \frac{1}{2}\,(B_i^r + B_{i+1}^r) \tag{3.5}$$

To calculate averages like (3.5) at the boundaries $r = 0$, $r = 1$ one needs two additional points $x_{-1/2}$ and $x_{N+1/2}$ which are defined analogous to (3.5):

$$x_0 = 0 = \frac{1}{2}(x_{1/2} + x_{-1/2})$$

$$x_N = 1 = \frac{1}{2}(x_{N+1/2} + x_{N-1/2})$$

The variables at these points are defined according to the proper boundary conditions.

3.1.2. *Boundary Conditions*

The origin $r = 0$: the requirement that all physical quantities are single-valued at the origin imposes some conditions. For any quantity $\mathbf{u}$ with an expansion like (3.1) this requirement writes

$$\left.\frac{\partial \mathbf{u}}{\partial \theta}\right|_{r=0} = 0.$$

Together with expressions like (3.5) this leads to the following boundary conditions at

$r = 0$ for the $\mathbf{u}_{mn}(r;t)$:

$$B^r_{i=0}(m \geq 2) = 0$$

$$V^r_{i=0}(m \geq 2) = 0$$

$$B^\theta_{-1/2}(m \geq 2) = -B^\theta_{1/2}(m \geq 2)$$

$$V^\theta_{-1/2}(m \geq 2) = -V^\theta_{1/2}(m \geq 2)$$

$$B^z_{-1/2}(m \geq 2) = -B^z_{1/2}(m \geq 2)$$

$$V^z_{-1/2}(m \geq 2) = -V^z{}_{1/2}(m \geq 2)$$

$$P_{-1/2}(m \geq 2) = -P_{1/2}(m \geq 2)$$

$$B^r_{i=0}(m = 0) = 0$$

$$V^r_{i=0}(m = 0) = 0$$

$$B^\theta_{-1/2}(m = 0) = -B^\theta_{1/2}(m = 0)$$

$$V^\theta_{-1/2}(m = 0) = -V^\theta_{1/2}(m = 0)$$

$$B^z_{-1/2}(m = 0) = +B^z_{1/2}(m = 0)$$

$$V^z_{-1/2}(m = 0) = +V^z{}_{1/2}(m = 0)$$

$$P_{-1/2}(m = 0) = +P_{1/2}(m = 0)$$

$$B^r_{i=0}(m = 1) = iB^\theta_{1/2}(m = 1)$$

$$B^\theta_{-1/2}(m = 1) = +B^\theta_{1/2}(m = 1)$$

$$V^r_{i=0}(m = 1) = iV^\theta_{1/2}(m = 1)$$

$$V^\theta_{-1/2}(m = 1) = +V^\theta_{1/2}(m = 1)$$

$$B^z_{-1/2}(m = 1) = -B^z_{1/2}(m = 1)$$

$$V^z_{-1/2}(m = 1) = -V^z{}_{1/2}(m = 1)$$

$$P_{-1/2}(m = 1) = -P_{1/2}(m = 1)$$

The outer boundary $r = 1$: in this work we assume that the boundary at $r = 1$ is an electrically conducting metal wall. This together with expressions like (3.5) results in the

following conditions:

$$
\begin{aligned}
B^r_N(m \geq 0) &= 0 \\
B^\theta_{N+1/2}(m \geq 0) &= B^\theta_{N-1/2}(m \geq 0)\ \frac{x_{N-1/2}}{x_{N+1/2}} \\
B^z_{N+1/2}(m \geq 0) &= B^z_{N-1/2}(m \geq 0) \\
V^r_N(m \geq 0) &= 0 \\
V^\theta_{N+1/2}(m \geq 0) &= V^\theta_{N-1/2}(m \geq 0)\ \frac{x_{N-1/2}}{x_{N+1/2}} \\
V^z_{N+1/2}(m \geq 0) &= V^z_{N-1/2}(m \geq 0) \\
P_{N+1/2}(m \geq 0) &= -P_{N-1/2}(m \geq 0)
\end{aligned}
$$

3.1.3. *Divergence Condition* $\nabla \cdot \mathbf{B} = 0$

The grid as defined in paragraph 3.1.1 allows to identically fulfill the vectoridentity

$$\nabla \cdot (\nabla \times \mathbf{u}) = 0$$

if one defines the divergence and curl operations as follows

$$(\nabla \cdot \mathbf{u}) = \left(\frac{1}{r}\frac{\partial(ru^r)}{\partial r} + \frac{1}{r}\frac{\partial(u^\theta)}{\partial \theta} + \frac{\partial(u^z)}{\partial z} \right)_{i+1/2}$$

$$
\begin{aligned}
(\nabla \times \mathbf{u})^r &= \left(\frac{1}{r}\frac{\partial(u^z)}{\partial \theta} - \frac{\partial(u^\theta)}{\partial z} \right)_i \\
(\nabla \times \mathbf{u})^\theta &= \left(\frac{\partial(u^r)}{\partial z} - \frac{\partial(u^z)}{\partial r} \right)_{i+1/2} \\
(\nabla \times \mathbf{u})^z &= \left(\frac{1}{r}\frac{\partial(u^\theta)}{\partial r} - \frac{1}{r}\frac{\partial(u^r)}{\partial \theta} \right)_{i+1/2}
\end{aligned}
$$

If this is done $\nabla \cdot \mathbf{B} = 0$ can be implemented as an initial-value condition because the evolution equation for $\mathbf{B}$ has the form

$$\frac{\partial \mathbf{B}}{\partial t} = \nabla \times \mathbf{u}$$

which means

$$\nabla \cdot \frac{\partial \mathbf{B}}{\partial t} = \frac{\partial \nabla \cdot \mathbf{B}}{\partial t} = \nabla \cdot (\nabla \times \mathbf{u}) = 0$$

and

$$\nabla \cdot \mathbf{B} = 0$$

always if this condition holds for $t = 0$. That is the way we handle this condition in our code.

3.2. Temporal Discretization

3.2.1. *TheAlgorithm*

The temporal advance of the MHD equations is performed through the Fourier coefficients as assumed in (3.1).

In our code we use the semi-implicit predictor-corrector scheme of Harned et al./1,2/. This scheme allows to circumvent the CFL conditions of explicit schemes for the fastest timescale, the fast compressible modes, without doing the timeadvance fully implicit. Thus we are not limited to a too small timestep typical of explicit schemes. Neither are we limited through the large matrix manipulations inherent in implicit schemes. The central idea is to make the fastest timescale implicit,/1/.

The algorithm is as follows,/2/:

$$\mathbf{B}_* = \mathbf{B}_n + \alpha \Delta t \mathbf{F}_1(\mathbf{B}_n, \mathbf{V}_n) \tag{3.6}$$

$$P_* = P_n + \alpha \Delta t F_2(P_n, \mathbf{V}_n) \tag{3.7}$$

$$V^z_{n+1} = V^z_n + \Delta t F_3(P_*, \mathbf{B}_*, \mathbf{V}_n) \tag{3.8}$$

$$\mathbf{V}^\perp_{n+1} - \mathbf{S}(\mathbf{V}^\perp_{n+1}) = \mathbf{V}^\perp_n + \Delta t \mathbf{F}_4(P_*, \mathbf{B}_*, \mathbf{V}_n) - \mathbf{S}(\mathbf{V}^\perp_n) \tag{3.9}$$

$$\mathbf{B}_{**} = \mathbf{B_n} + \Delta t \mathbf{F}_1(\mathbf{B}_*, \frac{1}{2}(\mathbf{V}_{n+1} + \mathbf{V}_n)\ ) \tag{3.10}$$

$$\mathbf{B}_{n+1} = \mathbf{B}_{**} + \Delta t \mathbf{F}_5(\mathbf{B}_{**}) \tag{3.11}$$

$$P_{n+1} = P_n + \Delta t F_2(P_*, \frac{1}{2}(\mathbf{V}_{n+1} + \mathbf{V}_n)\ ), \tag{3.12}$$

n, $n+1$ characterize the times t_n, t_{n+1} and (*,**) defines the predictor time in between. Furthermore we have:

$$\mathbf{F}_1 = \nabla \times (\mathbf{V} \times \mathbf{B})$$

$$F_2 = -\gamma P \nabla \cdot \mathbf{V} - \mathbf{V} \cdot \nabla P$$

$$F_3 = (-\mathbf{V} \cdot \nabla \mathbf{V} - \nabla P + (\nabla \times \mathbf{B}) \times \mathbf{B})^z$$

$$\mathbf{F}_4 = (-\mathbf{V} \cdot \nabla \mathbf{V} - \nabla P + (\nabla \times \mathbf{B}) \times \mathbf{B})^\perp$$

$$\mathbf{F}_5 = -\nabla \times (\eta \nabla \times \mathbf{B})$$

Without the semi-impliczit operator $\mathbf{S}(\mathbf{V}^\perp)$ and the special treatment of $\mathbf{v}^z$ the algorithm (3.6)-(3.12) would simply be a second order accurate predictor-corrector scheme if $\alpha = 0.5$. In general one choses $\alpha = 0.5 + \epsilon$ because one needs some numerical damping in order not to enhence numerical noise.

The operator $\mathbf{S}$ is chosen to make fastest timescale implicit but leaving the rest explicit. As $\mathbf{S}$ is not uniquely defined, we choose the following form ,/2/:

$$\mathbf{S} = (\Delta t)^2 A_0^2 \nabla(\nabla \cdot \mathbf{V}^\perp) \tag{3.13}$$

This form of the operator allows a large enough timestep and is extremely well suited for the staggered mesh as this operator just introduces a tridiagonal matrix problem to be solved. This can be done very efficiently.

In tokamak physics where a set of reduced equations exist which do not contain the fast compressible modes the semi-implicit method allows to treat the full MHD problem with the same amount of computing time once needed for the reduced equations. And the full MHD equations have to be solved because they contain more and important physics than the reduced equations.

3.2.2. *Numerical Smoothing*

The MHD equations allow singularities which have to be calculated on a finite numerical grid. Therefore one is forced to add some terms to the equations (2.1)-(2.4) to smoothen the singularities. The η-term helps to solve the problem for the magnetic field $\mathbf{B}$ but to solve the problem for the velocity $\mathbf{V}$ an additional viscosity term

$$\mu \nabla^2 \mathbf{V}$$

is used. If μ is kept small enough $\mu \sim \frac{\eta}{10}$ then this viscosity is just a numerical smoothing operator and it does change the physics qualitatively.

3.2.2. *Equilibria and Perturbations*

The simplest start configuration is an instable one-dimensional ideal equilibrium which is slightly perturbed. Such an equilibrium is defined by

$$f(r, \theta, z; t) = f(r)$$

$$\mathbf{V}(t = 0) = \mathbf{0}$$

This leads to the following equation for the equilibrium quantities

$$\frac{\partial P}{\partial r} = - \frac{B^\theta}{r} \frac{\partial (r B^\theta)}{\partial r} - B^z \frac{\partial B^z}{\partial r}. \tag{3.14}$$

One can choose two profiles and the third one is defined through (3.14). Defining the equilibrium current in z direction j_0^z and the safetyfactor $q(r)$

$$j_0^z = \frac{1}{r} \frac{\partial (r B^\theta)}{\partial r}$$

$$q(r) = rk \frac{B^z}{B^\theta}$$

one has various possibilities to define a suitable start configuration. The equilibrium is then perturbed

$$\mathbf{V} \sim \epsilon \, f(r)$$

with $f(r)$ an arbitrary function and $|\epsilon| \approx 10^{-8}, 10^{-7}$.

4. NUMERICAL TEST CALCULATIONS

In this chapter we do some calculation to demonstrate the performance of our code. Before doing some nonlinear calculations the following points have to be cleared.

1. It must be shown that $\nabla \cdot \mathbf{B} = 0$ as a function of time is in fact valid.
2. It must be demonstated that the code does not numerically dissipate energy.
3. It must be demonstrated that the code is able to reproduce the linear MHD theory very accuratly.

4.1. Numerical Performance

First we estimate the CPU-time necessary for a nonlinear run. For a first estimate of the CPU-time with a given number of gridpoints N_G, of Fourier modes N_F and of timesteps N_Z the following formula applies

$$t(CPU) \sim N_G \, N_Z \, (N_F)^b \, ,$$

where b is an empirical constant with $b \approx 1.6$.

For a typical nonlinear run the history of $\nabla \cdot \mathbf{B}(t)$ is shown in Fig.(1). The deviation of $\nabla \cdot \mathbf{B}$ from zero is small enough to be acceptable. As $\nabla \cdot \mathbf{B}$ is of order $O(10^{-11})$ it is at least four orders of magnitude smaller than the smallest parameter involved, namely μ which is of order $10^{-8} - 10^{-7}$.

The time evolution of the total energy for the same testcase is shown in Fig.(2). The total energy is constant in time at least on the time scale we usually work on. The figures (1),(2) prove that the code indeed satisfies the divergence condition and energy conservation which are some of the most important requirements one has to fulfill.

In paragraph 3.2.2. we introduced viscosity as a pure smoothing operator. Here we demonstrate that this operator indeed acts as numerical smoothing operator, if μ is small

enough.

It is well known /3/ that the instable ideal equilibrium

$$B^z = 1.$$

$$j^z = j_0(1-r^2)^2$$

with mode numbers $(m,n) = (1,1)$, $j_0 = \frac{2k}{q_0}$, $k = \frac{1}{5}$, $q_0 = q(r=0) = 0.73$ saturates into a nonlinear stable state with a singular current sheet, Fig.(3).

If we use this state as an initial configuration for a run with $\mu = 0$ then numerical errors are not dampened but tend to grow and the stable state is destroyed, Fig.(4). Setting $\mu = 7 \cdot 10^{-7}$ the stable initial configuration can be kept for quite a long time without changing the physics, Fig.(5). Fig.(4) corresponds to a time $t = 1000\tau_\alpha$, Fig.(5) to a time $t = 1000\tau_\alpha$.

4.2. Linear MHD

4.2.1. *Linear ideal MHD*

Our code is tested by comparing results with a well established linear eigenvalue code, /4/. This eigenvalue code can be used as a reference to numerical accuracy at least in the linear regime. The first test is ideal MHD. We consider the following ideal equilibrium

$$B^z = 1$$

$$q(r) = \frac{rkB^z}{B^\theta} = q_0 = const.$$

with modenumbers $(m,n) = (2,1)$ and $k = 0.2$. In radial direction 200 gridpoints are used. If one plots the linear growth rates λ against $q(r=0) = q_0$ this testcase can be used to establish how sensitiv the nonlinear initial value code is in the neighbourhood of the marginal point. We try to answer the question how large a growth rate must be to be resolved by our code or how accurate the marginal point can be resolved.

The marginal point is $q_0 = q_m = 1.9221$ with

$$q_0 < q_m \rightarrow stable$$

$$q_0 > q_m \rightarrow instable$$

The results are presented in Fig.(6). The growth rate λ is plotted against q_0 with

$$q_0 \in [1.9222, 2.03]$$

and the marginal point is indicated. This results show that we can resolve the marginal point . The deviations between the eigenvalue code and our code are so small that in Fig.(6) no error bars can be seen. The percentual deviation $\Delta\lambda$ is

$$0.001\% < \Delta\lambda < 0.65\%.$$

The resultes of both codes match to a very high accuracy.

4.2.2. *Linear resistive MHD*

In this case we consider an equilibrium which allows to demonstrate two different mechanisms for driving instabilities namely pressure and current driven modes, /4,5/. We consider tokamak like profiles

$$j^z(r) = j_0(1 - \frac{r^2}{a^2}),$$

$$B^z = 1 \ ,$$

$$\rho = 1$$

with $\frac{q(a)}{q(0)} = 2$ and $r^{surface} = a = 1$. If one guaranties $q > 1$ the $(m = 1)$-tearing mode is stable and the $(m = 2)$-tearing mode is the most dangerous instability. This mode is the unstable for $2.20 \leq q(a) \leq 4.0$. In Fig.(7) the growth rate λ is plotted against $q(a)$. For $nq(a) < 2.3$ one has pressure-driven modes and for $nq(a) > 2.3$ the modes are current-driven. The transition near $nq(a) \approx 2.3$ is clearly visible.

As in paragraph 4.2.1. no errorbars are plotted because the percentual deviation $\Delta\lambda$ between the codes is too small

$$\Delta\lambda < 0.5\%.$$

We used 200 gridpoints and the resitivity η is $\eta_0 = const. = 10^{-5}$, in the eigenvalue code and in the nonlinear code $\eta(r_s) = 10^{-5}$ where r_s defines the singular surface.

4.3 Nonlinear resistive MHD

After demonstrating the performance of our code in the well known linear regime we consider now a nonlinear application as a nonlinear testcalculation.

As a first step we reproduce the well known nonlinear saturation of the ideal (m=1) internal kink, /3/. Fig.(8) shows the contourplots of the plasma pressure and the current and Fig.(9) shows the radial profiles of the pressure and the current obtained by a quasi-nonlinear calculation, where just the (m=1,n=1) and no higher harmonics are retained. Figs.(10,11) show the result of the same calculation with 10 harmonics. It is obvious that the quasinonlinear calculation in this case is an excellent approximation.

Due to the singular current sheet this ideal nonlinear equilibrium should be extremly unstable to resistive modes. So we use this configuration as an initial configuration for resistive $(m = 1)$ calculations. We expect the decay of the singular current layer and we follow the evolution of the $(m = 1)$ instability.

Furthermore this calculation models Kadomtsev's picture of the sawtooth crash,/6/, especially the final step of the reconnection process. Our two-step calculation illustrades the different steps which finally lead to the reclosing of the lines of force. Kadomtsev's argumentation is as follows,/6/. Starting with the nonlinear analysis of the ideal internal kink /3/ which shows that the weak ideal instability leads to the formation of a thin layer with fields which are opposite in direction, i.e. between which there is an infinite current density, Figs.(9,11), Kadomtsev argues that such a singular layer cannot exist in medium with finite resistivity. Finite resistivity leads to fieldline reconnection. Kadomtsev

estimates the total time for the reclosing process as

$$t \sim \eta^{-1/2}.$$

The $\eta^{-1/2}$ scaling can be verified if we use the nonlinear ideal equilibrium, Figs.(8,10), as an initial configuration for the resistive calculations. Fig.(12) shows a double logarithmic plot of $t = t(\eta)$. Assuming $t \sim \eta^a$ we find $a = -\frac{1}{2}$. Having shown the validity of the Kadomtsev picture in the above model with monotonic current profiles we conclude that the code described in this report can be considered a valuable tool to solve the resistive MHD equations in cylindrical geometry. Problems in fusion theory which can be handled in the framework of the straight tokamak model can be solved numerically with this code.

Acknowledgements

I thank Dr D. Biskamp for providing me with a first draft of the code, Dr W. Kerner for constant advice in numerical methods and problems, especially in how to test codes very accurately. Dr D.S. Harned for explaining and discussing his semi-implicit method, H. Welter for valuable advice concerning programming techniques and the handling of such a code, M. Walter for helping me in various ways. Last but not least I would like to thank K. Lerbinger for many important discussions and his constant interest in my work.

REFERENCES

/1/

D.S.Harned, W.Kerner

IPP-Report 6/234, March 1984

/2/

D.S.Harned, W.Kerner

Nuclear Science and Engineering,92, 119-125,(1986)

/3/

M.N.Rosenbluth, R.Y.Dagazian, P.H.Rutherford

Phys. Fluids,16, 1984-1902, (1973)

W.Park, D.A.Monticello, R.B.White, S.C.Jardin

Nuclear Fusion, 20, 1181-1185, (1979)

/4/

W.Kerner, K.Lerbinger, R.Gruber, T.Tsunematsu

Comp. Phys. Comm., 36, 225-240 (1985)

/5/

W.Kerner, A.Jakoby, K.Lerbinger

J. Comp. Phys., 66, 332-355, (1986)

/6/

B.B. Kadomtsev

Fiz Plazmy, 1, 710(1975)

FIGURE CAPTIONS

Fig (1)

$\nabla \cdot \mathbf{B}$ as a function of time for a typical nonlinear calculation. The time is measured in units of τ_α.

Fig (2)

The total energy as a function of time for a typical nonlinear calculation. The time is measured in units of τ_α.

Fig (3)

The nonlinear equilibrium according to Ref.(3),

(a) pressure, (b) current density.

Fig (4)

Further evolution of the nonlinear equilibrium of Fig.(3) with $\mu = 0$, i.e. without viscosity.

Fig (5)

Further evolution of the nonlinear equilibrium of Fig.(3) with $\mu = 7 \cdot 10^{-7}$, i.e. with viscosity.

Fig (6)

Testcase ideal MHD.

Growth rate λ vs q_0. The marginal point is indicated.

Fig (7)

Testcase resistive MHD.

Growth rate λ vs q_0. The transition point with $nq(a) \approx 2.3$ is indicated.

Fig (8)

Contour plots of the quasinonlinear calculation.

(a) Pressure, (b) Current density

Fig (9)

Radial cuts along the symmetry axis

(a) Pressure, (b) Current density

Fig (10)

The same as Fig.(8) but with 10 harmonics.

(a) Pressure, (b) Current density

Fig (11)

The same as Fig.(9) but with 10 harmonics.

(a) Pressure, (b) Current density

Fig (12)

Double logarithmic plot of $t = t(\eta)$ to prove the Kadomtsev theory of the sawtooth.

$\eta = 10^{-6}, 10^{-5}, 10^{-4}$, t =reclosing time.

Figure (1)

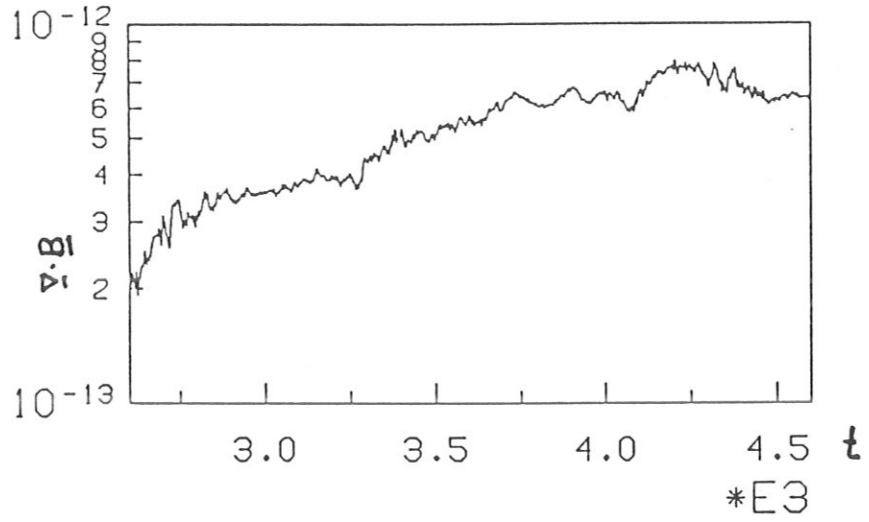

Figure (2)

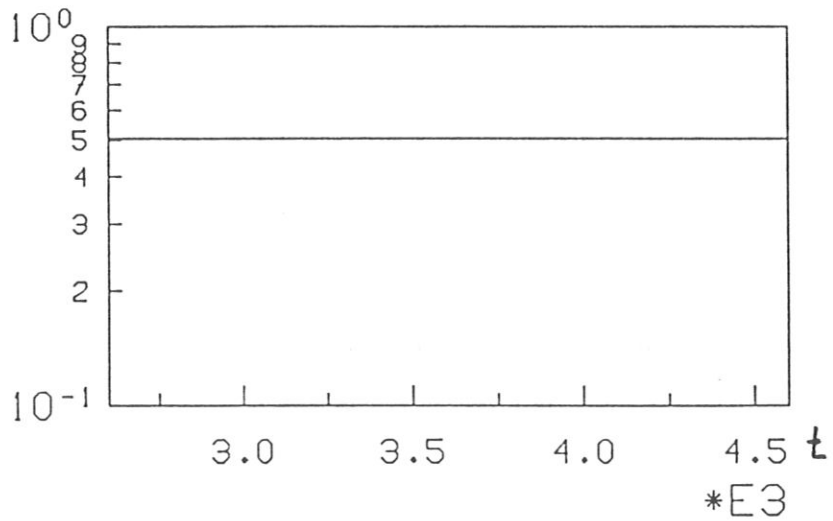

Figure (3)

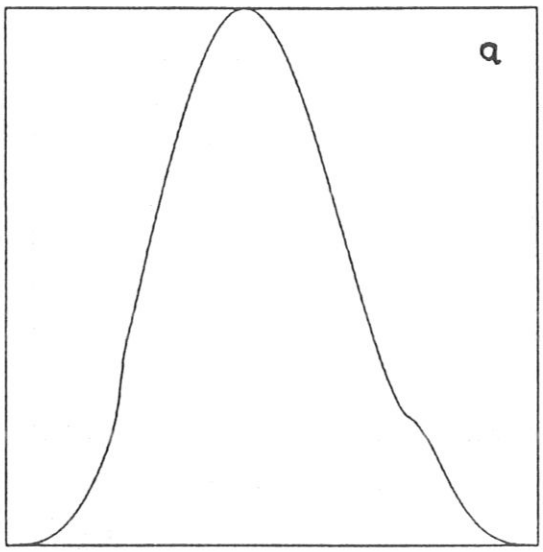

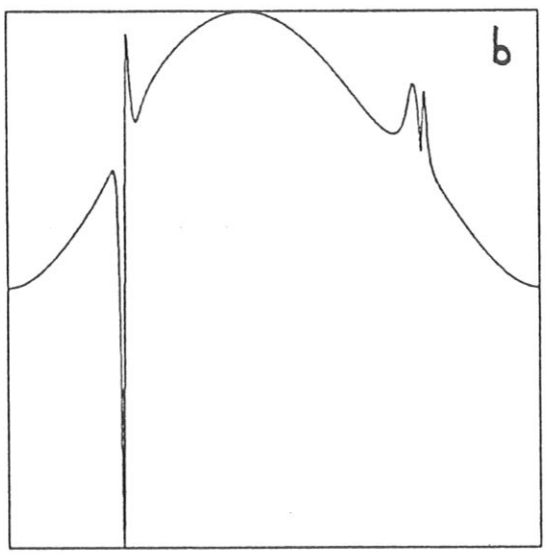

Figure (4)

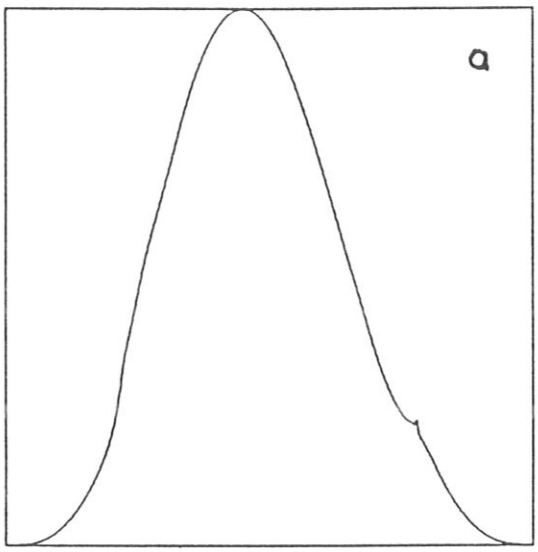

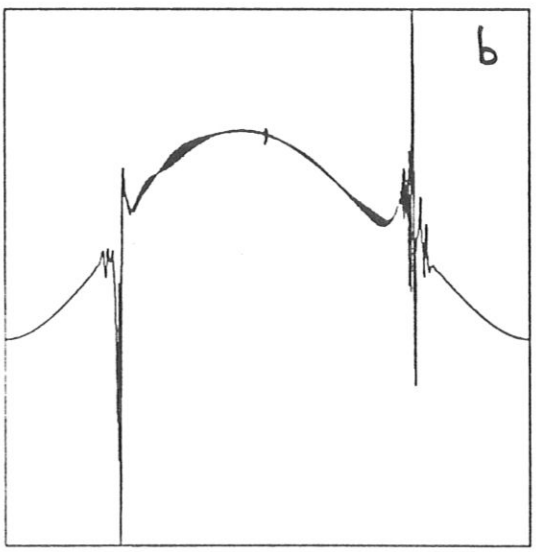

Figure (5)

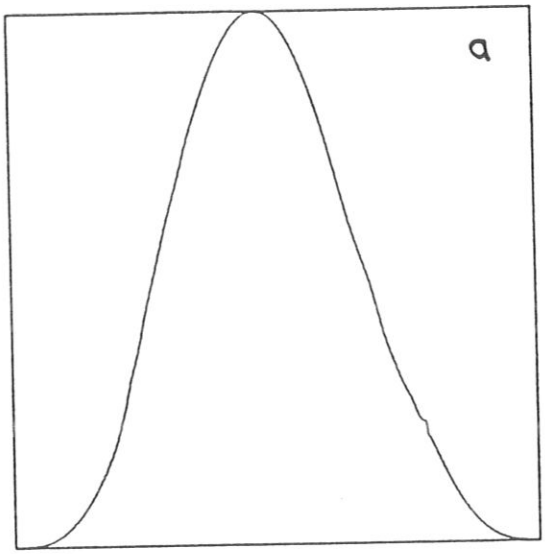

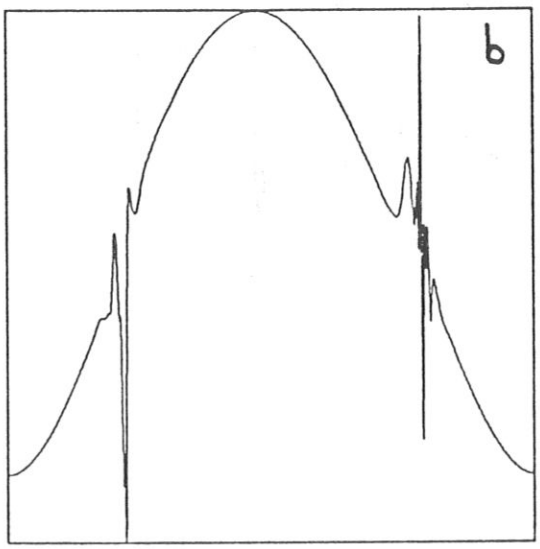

Figure (6)

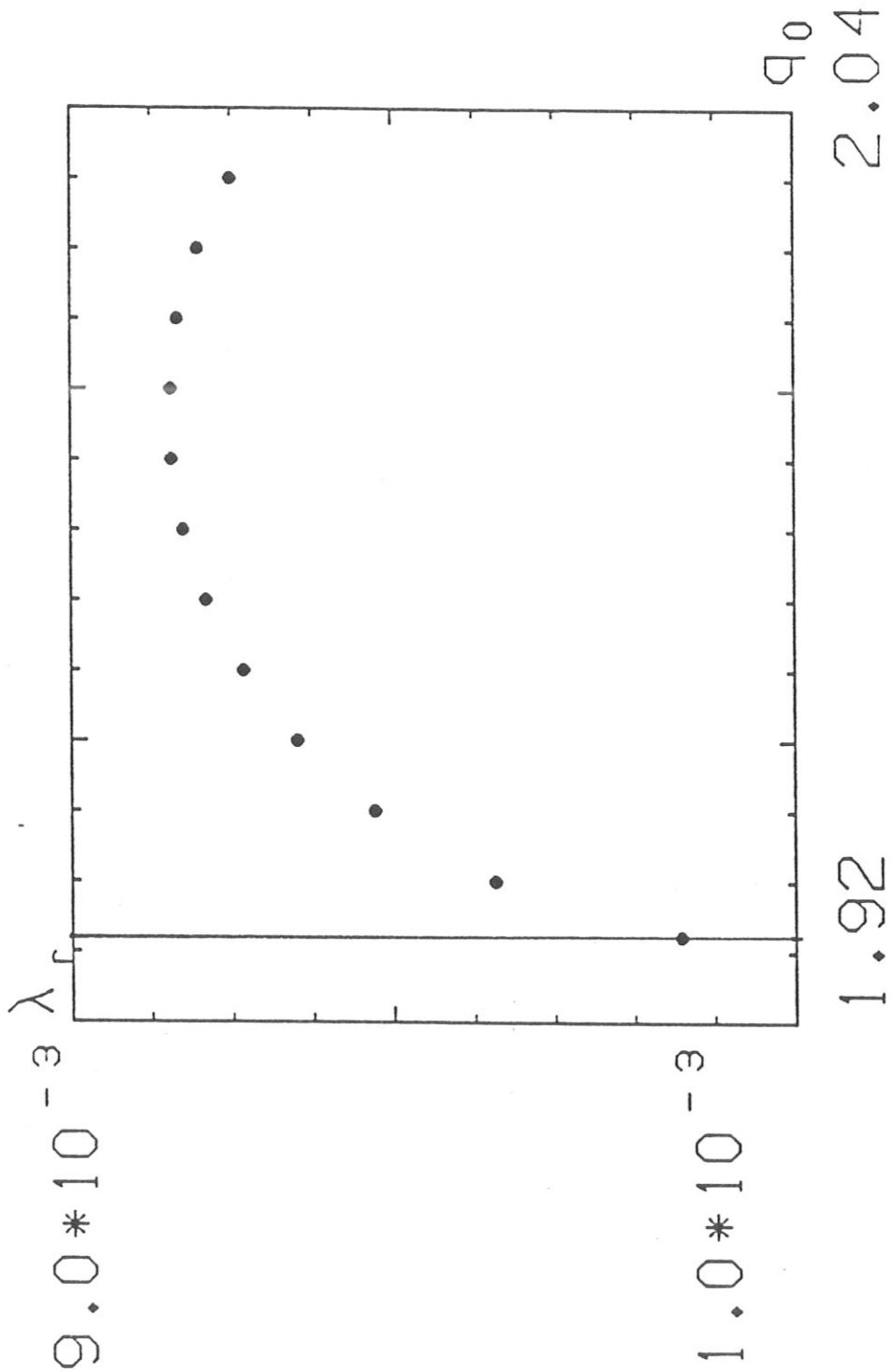

Figure (7)

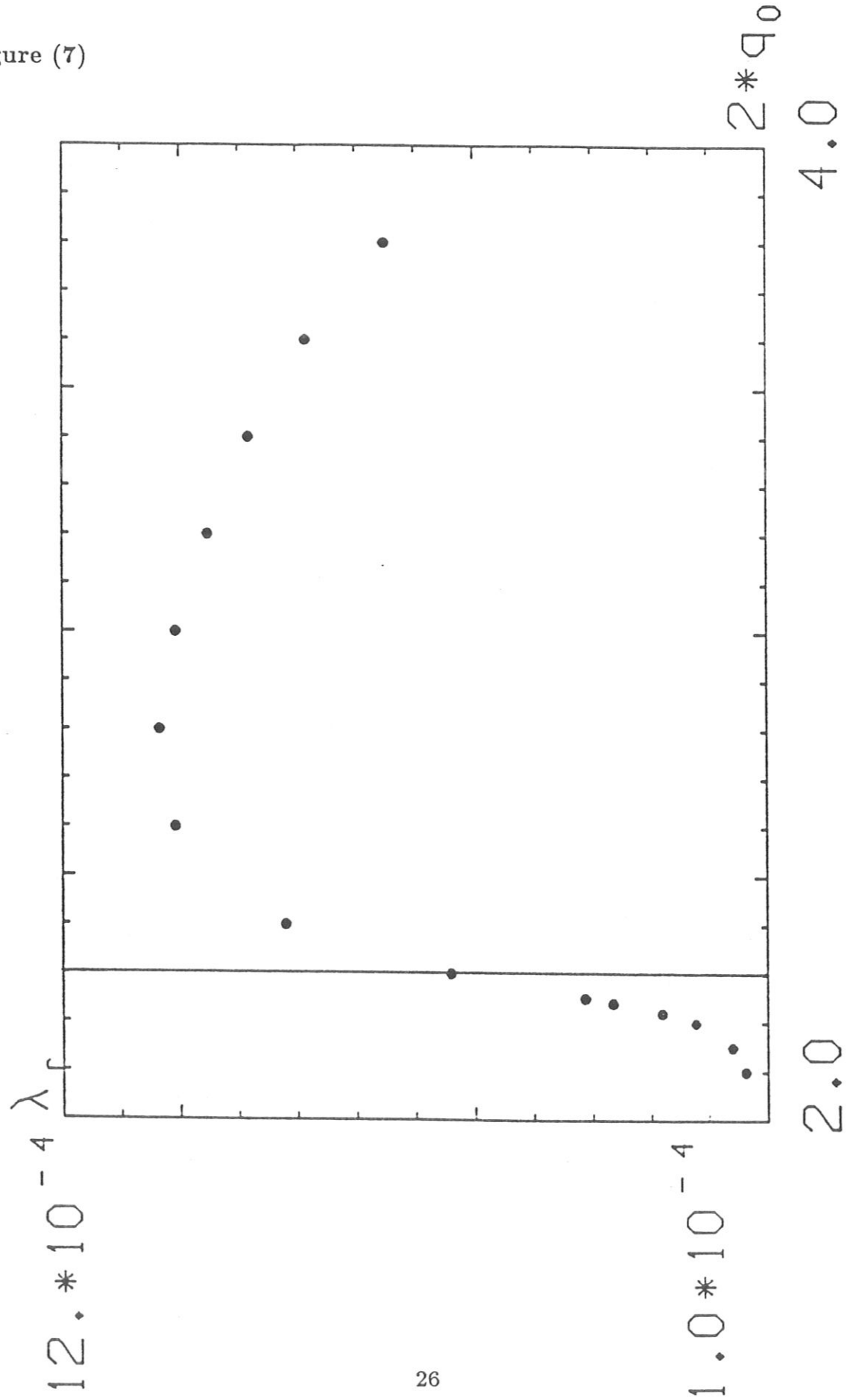

Figure (8)

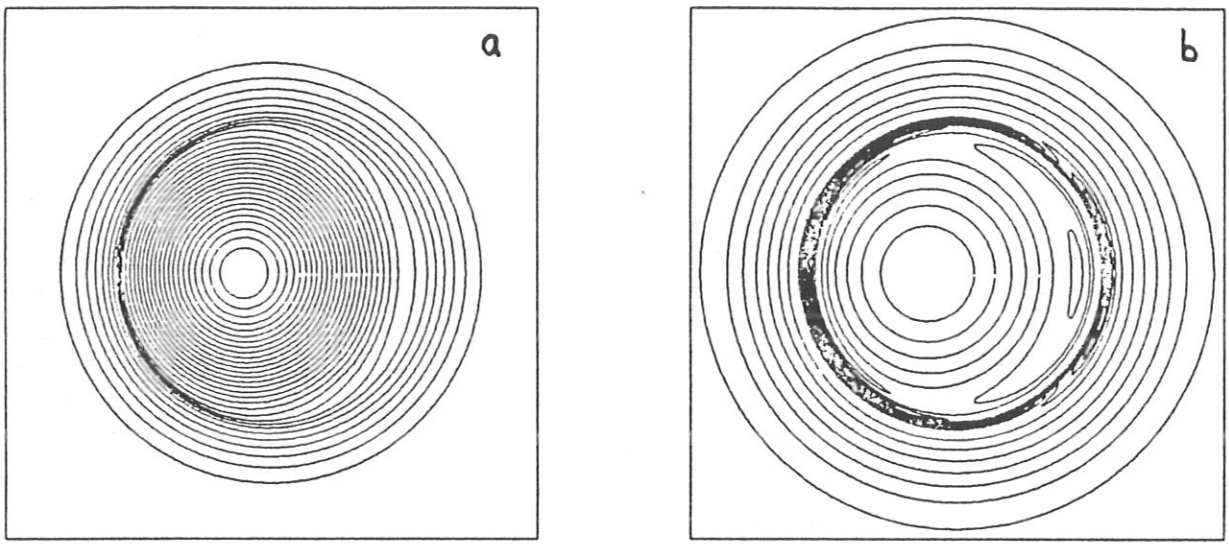

Figure (9)

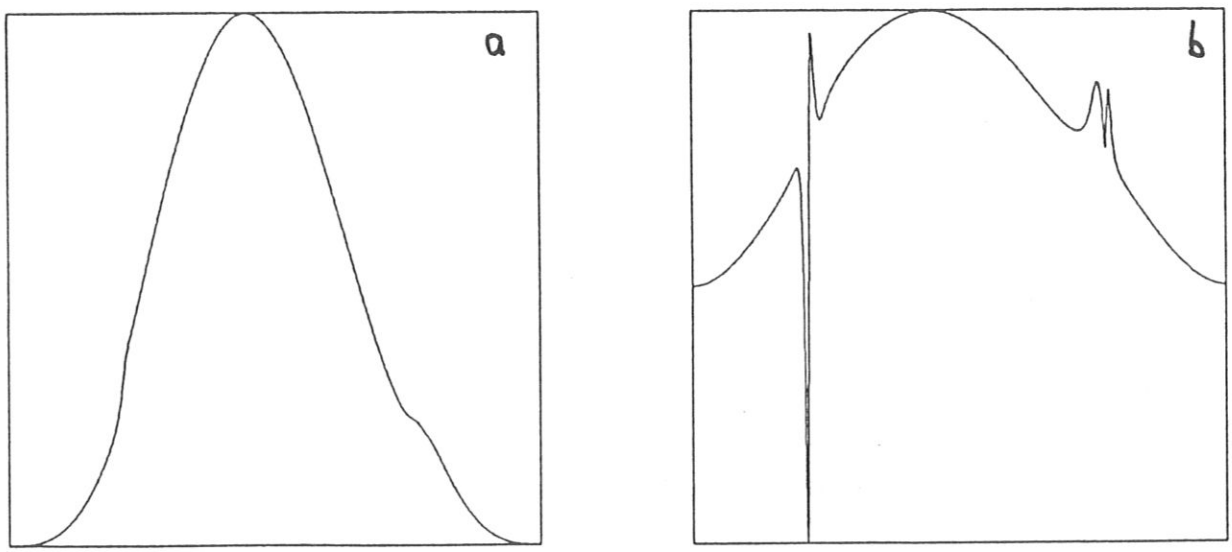

Figure (10)

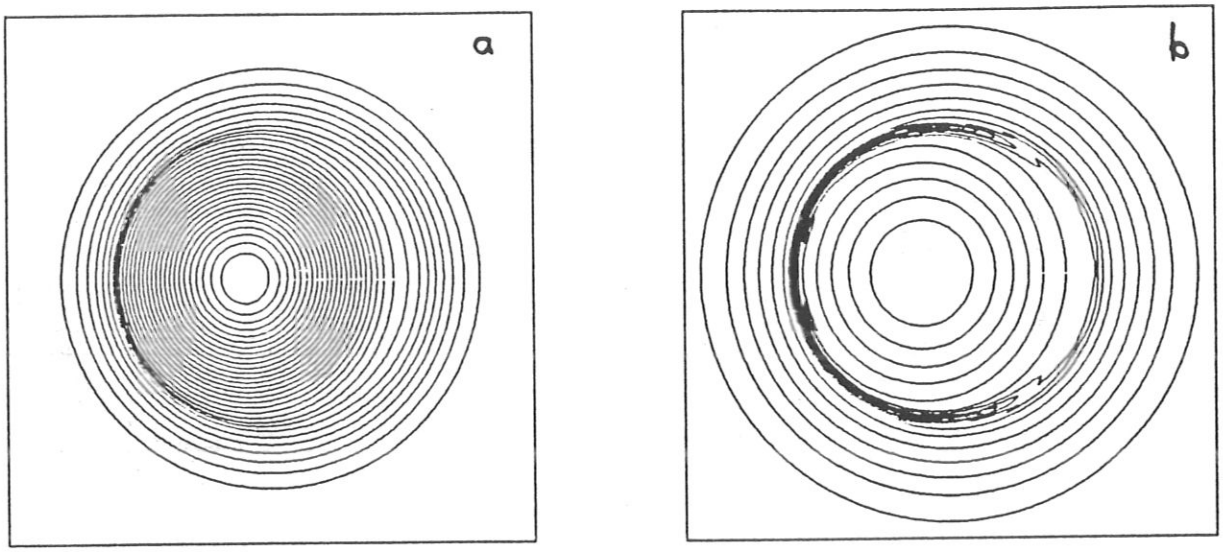

Figure (11)

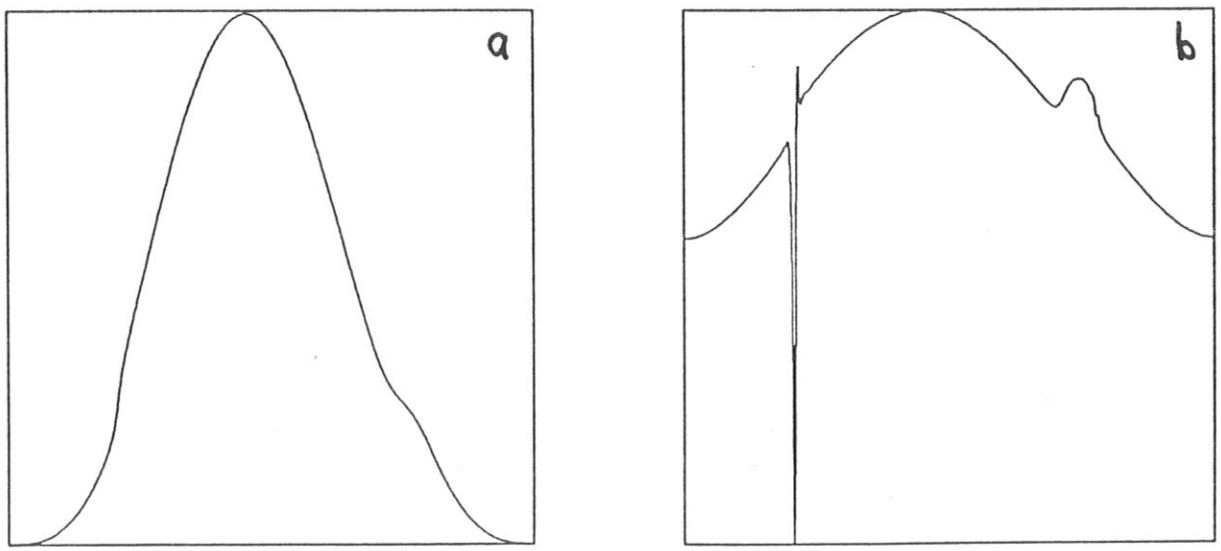

Figure (12)